Full Length Article

Pore structure of mesoporous silica (KIT-6) synthesized at different temperatures using positron as a nondestructive probe

B. Zhou [a], C.Y. Li [b], N. Qi [a,*], M. Jiang [c], B. Wang [a], Z.Q. Chen [a,*]

[a] *Hubei Nuclear Solid Physics Key Laboratory, Department of Physics, Wuhan University, Wuhan 430072, China*
[b] *College of Electric Power, North China University of Water Resources and Electric Power, Zhengzhou 450045, China*
[c] *Key Laboratory of Neutronics and Radiation Safety, Institute of Nuclear Energy Safety Technology, Chinese Academy of Sciences, Hefei 230031, China*

ARTICLE INFO

ABSTRACT

Ordered mesoporous SiO_2 (KIT-6) was synthesized using triblock copolymer P123 as the structure template and tetraethyl orthosilicate (TEOS, $C_8H_{20}O_4Si$) as silica source. Small-angle X-ray scattering and high resolution electron microscope measurements indicate the 3d cubic Ia3d symmetry of the pore structure of KIT-6 synthesized at 30–120 °C. When the synthesis temperature increases to 180 °C, the order of pores was deteriorated. The pore size was estimated by nitrogen adsorption/desorption measurements, which increases from 3.8 nm to 18.5 nm as the synthesis temperature increases from 30 °C to 180 °C. With the increase of mesopore size, the pore wall thickness shows continuous decrease. Positron annihilation lifetime spectra was measured for the synthesized KIT-6. The lifetime spectra can be resolved to two short and two long lifetime components. The two long lifetimes τ_3 and τ_4 correspond to o-Ps lifetime in micropore and mesopores, respectively. The size of mesopores was estimated from the o-Ps lifetime by using Goworeck's model for cylindrical pores, which shows continuous increase with synthesis temperature, and is consistent with the N_2 adsorption/desorption measurements. The size of micropore has no change with increasing synthesis temperature. However due to the decrease in wall thickness, the number of micropores in the wall shows subsequent decrease. In addition, the second lifetime component τ_2 is also found to be a sensitive parameter for the pore size, which shows the same trend as lifetime τ_4 with increasing synthesis temperature.

© 2018 Published by Elsevier B.V.

1. Introduction

In the last decades, mesoporous material has attracted much attention due to their wide applications in many fields, such as adsorption, separation, catalytic reaction, drug deliver, sensors, low-k dielectrics, energy storage and so on [1–4]. Among the mesoporous materials, silica-based materials were most frequently studied because of their tunable pore size, large surface area and controllable structure [5–9]. A series of mesoporous silica, such as MCMn, SBAn, FDUn, KITn, etc. have been synthesized by different templating schemes [7,10–13]. KIT-6 silica has bicontinuous cubic structure of Ia3d symmetry and contains interpenetrating cylindrical pores, which is more suitable for the hard template and support of catalysts [14]. It was shown that the pore size of mesoporous silica could be controlled through delicate regulation of the reaction temperature, surfactant type or concentration, and swelling agent concentration [5,7]. The pore structure of other

mesoporous materials synthesized by hard-templating method can thus be controlled by adjusting the pore diameter of the templates. Therefore, it is important to tailor the pore size of KIT-6 in order to produce more abundant target materials.

Comparing with the tuning of pore size, characterization of the pore size and pore structure of the porous material is more important. Different techniques have been used to measure pore size and pore structure. The most popular methods are small-angle X-ray scattering (SAXS), gas adsorption/desorption and high-resolution transmission microscopy. SAXS can provide the unit cell dimensions and is more effective for materials with long range order. Gas adsorption/desorption provides information on pore size, pore volume, and surface area, but it is mainly effective for open mesopores. It cannot detect the closed-pores. High-resolution transmission microscopy is a powerful tool to elucidate the pore geometry. It is desirable to have more experimental techniques which can provide more comprehensive information about the pore size and pore structure.

Positron annihilation spectroscopy (PAS) has been widely used to study vacancy defects in various materials such as metal and

alloys, semiconductors, polymers and porous materials [15–17]. Positrons will be preferentially trapped by vacancy-type defects such as monovacancies, divacancies, vacancy clusters and voids. Due to a lower electron density, the positron will live much longer at vacancy sites. In many porous materials, positron will also combine one electron to form a metastable hydrogen-like atom called positronium (Ps), which has a radius of 1.06 Å and binding energy of 6.8 eV. According to quantum mechanics, positronium can have either the spin anti-parallel para-positronium (p-Ps) (S = 0, m_s = 0) or the spin parallel ortho-positronium (o-Ps) (S = 1, m_s = 0, ±1). In vacuum, the positronium will undergo self annihilation. The self-annihilation lifetime of p-Ps via 2γ-annihilation is 125 ps, while that of o-Ps via 3γ-annihilation is 142 ns. The ratio of p-Ps to o-Ps formation probability is 1:3.

When positronium is formed in porous materials, it will be localized in the pores. Due to the very short lifetime, p-Ps is weakly affected by the surrounding environment. However, the o-Ps has relatively much longer lifetime, then it will move around and collide with the pore wall back and forth. During the collision, it has chance to pick off one electron from pore wall and undergo 2γ-annihilation [18]. The pick-off annihilation lifetime of o-Ps will be reduced to a few ns, which depends on the pore size. A semi-empirical relationship between o-Ps lifetime and pore size R was established by Tao and Eldrup et al. [19,20] assuming that positronium is trapped in a spherical pore, which can be expressed as follows:

$$\tau_{o-Ps}^{-1} = 2\left[1 - \frac{R}{R+\Delta R} + \frac{1}{2\pi}\sin\left(2\pi\frac{R}{R+\Delta R}\right)\right]. \tag{1}$$

where ΔR is the thickness of the electron layer on the surface of pores which is determined to be 1.656 Å for many materials, and was also suggested to be 1.8 Å for silica [21–23]. The above equation is based on spherical pores, and for pores with irregular shape, we can get equivalent dimension of the pores, such as the radius of cylinder, length of the cube and so on.

The above Tao-Eldrup model works for micropores with diameter less than 2 nm (corresponding to o-Ps lifetime $\sim 20ns$). For larger pores, the chance of positron to pick electron from the wall is reduced, so the self-annihilation of o-Ps should be considered. There are many modified models to evaluate pore size from the o-Ps lifetime for large pores [24,21,25]. In addition, Goworeck [26] also extended Tao-Eldrup models to correlate o-Ps lifetime with pore size for the cylindrical pores. Therefore those well established models enable positronium to be a good probe for evaluation of pores in a wide size range covering micropores and mesopores. On the other hand, the intensity of o-Ps lifetime component can also reflect the relative number of pores. Moreover, it is worth noting that positronium probe is not limited to open pores, it can also detect any closed pores. Thus positronium probe can provide more comprehensive information about the pore structures than other methods [27–32].

It should be noted that the formation and annihilation of o-Ps is also affected by other factors such as the chemical environment on the wall of the pores [33]. Some chemical agent will cause quenching of o-Ps lifetime and most of the time also prohibit positronium formation. If there are paramagnetic molecules in the surrounding of the pore, spin conversion of positronium will also occur, which causes decrease of both o-Ps lifetime and its intensity, since some o-Ps are converted to p-Ps and then annihilate by 2γ emission. Those chemical quenching and spin conversion will bring uncertainties in evaluating the pore size and pore volume. In addition, the positronium formation is forbidden in porous materials which are electrically conductive [34]. If the positronium formation is forbidden, we will even fail to probe the pore structure through o-Ps

lifetime. Jean et al. [35] proposed a new idea to measure the free volume size in polymer materials by using the second lifetime component. This is the positron annihilation lifetime in free volume holes without formation of positronium. They have successfully extended the Tao-Eldrup equation to measure the free volume hole with radius R < 5 Å by using τ_2. For free volume hole radius > 5 Å, their equation is no longer applicable and should be further modified. But this give hints that the positron lifetime τ_2 can be also used to detect the pores in porous materials.

In this paper, we synthesized the mesoporous KIT-6 template at different temperatures from 30 °C to 180 °C. The pore structure was studied by positron lifetime spectroscopy together with SAXS, HRTEM and N_2 adsorption/desorption measurements. Our results show that positronium is a very sensitive probe for not only mesopores but also micropores, and the mesopore size increases with increasing synthesis temperature. The second lifetime component τ_2 can be also used to detect the pore size.

2. Experiment

2.1. Sample preparation

KIT-6 was synthesized following the procedures from literature [13]. 6 g amphiphilic triblock copolymer Pluronic P123 (Mw = 5800, EO_{20}-PO_{70}-EO_{20}, Sigma Aldrich), 11.8 g hydrochloric acid and 6 g butanol were dissolved in 217 g of deionized water under stirring at 35 °C. After stirring for 4 h, 12.9 g tetraethyl orthosilicate (TEOS, $C_8H_{20}O_4Si$) was added into the above solution and it was stirred again at 35 °C for 24 h to ensure that the solution was distributed homogenously. The resulting solution was transferred into a Teflon-lined autoclave and kept at different temperatures for 24 h under static conditions. The product was filtered and dried at 100 °C. After that, the samples were further calcined at 550 °C for 5 h in air.

2.2. Characterization

Small-angle X-ray scattering patterns were measured by using an X-ray diffractometer (X'Pert Pro, PANalytical, Netherlands) with CuK_α radiation and the scanning angle 2θ was from 0.5 to 8° with the step of 0.026°. High resolution transmission electron microscopy image was obtained using a JEM-2010FEF microscope with an acceleration voltage of 200 kV. N_2 adsorption/desorption measurements were performed at 77 K by using a Micromeritics ASAP 2020 gas-sorption analyzer. Pore size distribution was estimated using the Barrett-Joyner-Halenda (BJH) method [36].

A conventional fast–fast coincidence lifetime spectrometer with time resolution of 280 ps was used for positron lifetime measurement. The sample were grinded and pressed to pellets under a static pressure of 6 MPa for 5 min before the measurement. $^{22}NaCl$ with 10 μCi activity was used as positron source, which was deposited between two 7.5 μm Kapton foils. The source was sandwiched between two pellet samples and was put into a vacuum chamber. The measurement was carried out under continuous vacuum pumping and the vacuum is kept at about 1×10^{-5} Torr. In order to collect the 3γ annihilation events of o-Ps in pores, the lower energy window on the discriminator for the stop signal was set to minimum and the range of time-to-amplitude converter was set to 200 ns. Each spectrum consists of 4096 channels of data with time scale of 50.3 ps/channel. A total count of 1×10^6 was collected for each lifetime spectrum, and two spectra were measured for each sample to verify the stability of the lifetime spectrometer.

3. Results and discussion

3.1. SAXS measurements

Fig. 1 shows the small angle X-ray scattering patterns of KIT-6 obtained under different hydrothermal reaction temperature. For the sample synthesized between 30 and 120 °C, all the SAXS patterns show the cubic Ia3d symmetry with two main peaks indexed as (2 1 1) and (2 2 0). This indicates the long range ordering of the pores in KIT-6. All the peaks shift to lower 2θ values with increasing synthesis temperature, which indicate the enlargement of
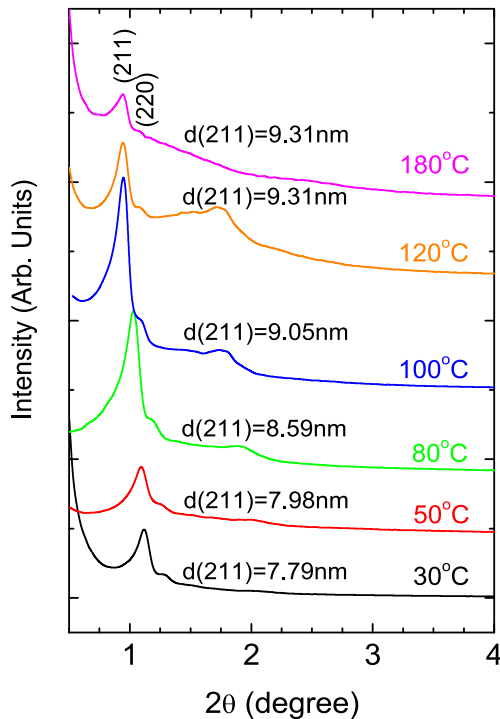

Fig. 1. Small angle X-ray scattering of KIT-6 synthesized at different hydrothermal temperatures.

mesopore structure. The peak intensities first show increase and then decrease when the synthesis temperature is higher than 100 °C. This suggests that the ordering of the pores synthesized at 100 °C is the highest. When the synthesis temperature is raised to 180 °C, the main (2 1 1) peak is much weaker, indicating that the long range order of pores is destroyed.

The plane spacing d_{211}, which is the periodic interval of pores (pore width + pore wall) of KIT-6, can be obtained according to the Bragg's equation:

$$2d \sin \theta = k\lambda \tag{2}$$

By using the 2θ value of the (2 1 1) peak in the above equation, the pore interval increases from 7.79 nm to 9.31 nm with the increasing synthesis temperature from 30 °C to 120 °C. This parameter was also labeled in Fig. 1. Since the (2 1 1) peak intensity is much weaker when the synthesis temperature is 180 °C, the pore interval for this sample may be unreliable.

3.2. HRTEM measurement

The HRTEM images for KIT-6 synthesized at different temperatures are shown in Fig. 2. The ordered pores can be clearly seen for the samples synthesized between 30 °C and 120 °C. The increase of pore size with synthesis temperature can be also observed. At 30 °C, the pore interval is about 7.7 nm, and it increase to about 10 nm when the temperature increase to 120 °C. This is in good agreement with the SAXS measurements. However, when the synthesis temperature increases to 180 °C, the pore ordering becomes weaker, and some pores agglomerate and form much larger pores. This suggests slight collapse of the pore structure. From the HRTEM images, it can be seen that the wall thickness decreases dramatically with increasing synthesis temperature, which has been also reported by others [37,38]. Especially at high temperature of 180 °C, the pore wall becomes very thin. This might be the reason for the collapse of pores.

3.3. N2 adsorption/desorption measurement

In order to obtain more details about pore structures such as pore size, pore volume, and specific surface area, the nitrogen adsorption/desorption measurement was also performed. The adsorption isotherms for KIT-6 synthesized at different temperatures are
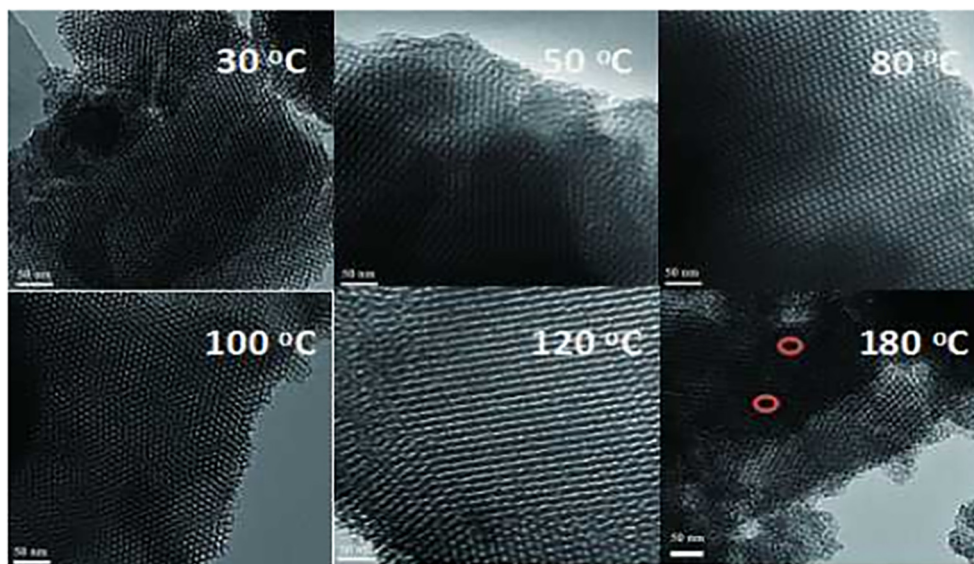

Fig. 2. High resolution transmission electron microscope image of KIT-6 synthesized at different hydrothermal temperatures.

shown in Fig. 3(a). The N$_2$ adsorption/desorption isotherms all show type IVa curves with H$_1$ hysteresis loops, according to the recent classification of IUPAC [39]. The capillary condensation occurs at a relative pressure P/P$_0$ of 0.6–1.0 [39–41]. These adsorption isotherm curves indicate that all the samples are mesoporous. The relative pressure P/P$_0$ of the capillary condensation shifts to higher value with the increase of synthesis temperature, which suggests increase of pore radius. At temperature of 180 °C, the relative pressure P/P$_0$ is about 1. This shows the existence of large pores.

The pore size distributions were calculated from the adsorption branches by using the Barrett-Joyner-Halenda (BJH) model [36], which are shown in Fig. 3(b). The average pore size D_p increases from 3.88 nm to 8.95 nm with the increase of synthesis temperature from 30 °C to 120 °C. The pore size distribution is relatively narrow, indicating that these samples have uniform pore sizes. When the sample was synthesized at 180 °C, the average pore size increases to 18.57 nm, and the pore size distribution becomes much broader. This might be due to the collapse of the pore structure and agglomeration of pores. All these results are consistent with the SAXS and HRTEM measurements.
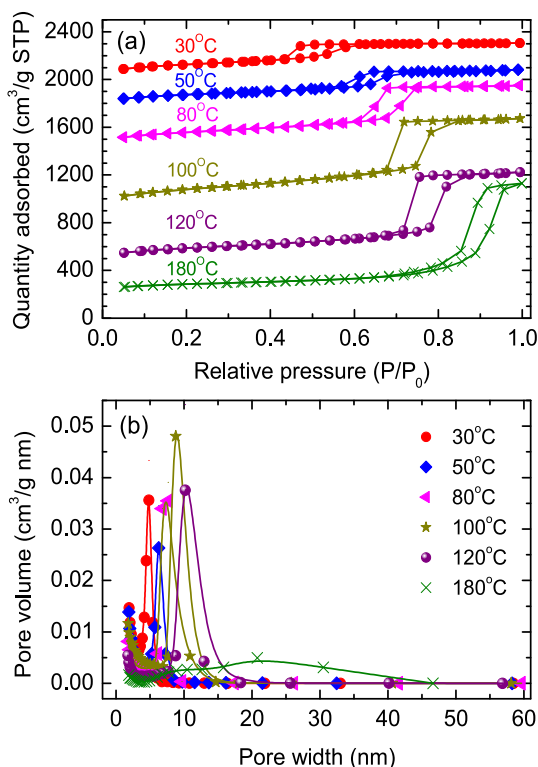

Fig. 3. (a) Nitrogen sorption isotherms and (b) pore size distribution of KIT-6 synthesized at different hydrothermal temperature.

We can get more detailed information about pore structure from the nitrogen adsorption/desorption measurements, such as the pore volume V_p and specific surface area S_{BET}. All the detailed results are listed in Table 1. The specific surface area increases at first and then decreases with the increase of the synthesis temperature. The sample prepared at 100 °C has the largest specific surface area of 763.5 m^2 g^{-1}. Furthermore, the pore volume increase from 0.57 cm^3 g^{-1} to 1.44 cm^3 g^{-1} as the synthesis temperature increases from 30 °C to 180 °C. The wall thickness was further estimated by the difference between pore interval and pore size. The wall thickness is about 3.91 nm for the sample synthesized at 30 °C, and it decreases drastically to 0.36 nm at 120 °C. For samples synthesized at 180 °C, the wall thickness is not available, since the pore size might be overestimated from the N$_2$ adsorption curve. In the above HRTEM results, we can clearly observe the decrease of wall thickness with increasing synthesis temperature. Especially for the sample synthesized at 180 °C, the thickness is very small, so the collapse of the ordered pore structure is rather easy to happen. The decrease of wall thickness with the increase of hydrothermal reaction temperature is due to the increase of hydrophobicity of the EO block and the decrease in the average length of EO segments, which were associated with the silica wall [5].

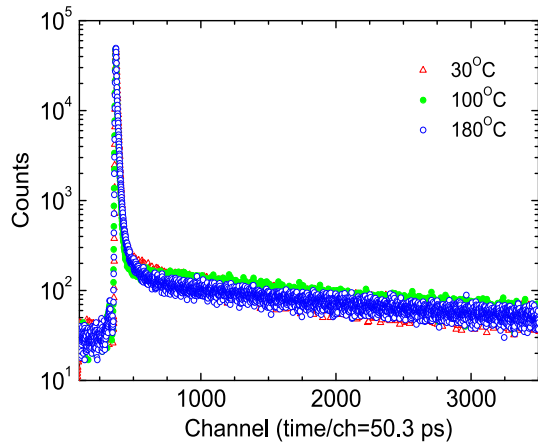### 3.4. Positron annihilation measurement

Fig. 4 shows the peak-normalized positron lifetime spectra measured for KIT-6 synthesized at temperature of 30 °C, 100 °C and 180 °C. The long tail in the lifetime spectrum suggests that there is a very long lifetime component in all the samples. This indicates the existences of large pores in these samples. The ideal positron lifetime spectrum is a sum of several exponential decay terms as follows:

$$L(t) = \sum_{i=1}^{N} \frac{I_i}{\tau_i} exp\left(-\frac{t}{\tau_i}\right),$$ (3)

where N is the number of lifetime components, and I_i is the corresponding intensities for each component. The ideal lifetime spectrum expressed by Eq. (3) is further convoluted with the time resolution $R(t)$ of the lifetime spectrometer:

$$Y(t) = L(t) * R(t) = N_t \sum_{i=1}^{N} \frac{I_i}{\tau_i} \int_0^{\infty} R(t - t') exp\left(-\frac{t}{\tau_i}\right) dt' + B,$$ (4)

where N_t is the total counts of the spectrum, B is the background count in the spectrum. All the positron lifetime spectra measured for KIT-6 samples can be resolved to four lifetime components by PATFIT program [42] according to the above equation. The shortest lifetime τ_1 is about 150 ps, which is attributable to p-Ps annihilation [43] and free positron annihilation. The second lifetime τ_2 varies from 549 ps to 619 ps in these samples, which is the annihilation lifetime of positrons trapped in micropores or larger mesopores.

Table 1
Textural characterization of KIT-6 synthesized at different hydrothermal temperatures. The plane spacing d$_{211}$ are calculated from the 2θ value of (2 1 1) peak by using Eq. (2). The specific surface area S$_{BET}$, pore volume V$_P$ and pore size D$_p$ are obtained from N$_2$ adsorption/desorption measurements, and the pore wall thickness d$_s$ is estimated from the difference between d$_{211}$ and pore size D$_p$)

Sample	d$_{211}$ (nm)	S$_{BET}$ (m^2/g)	V$_p$ (cm^3/g)	D$_p$ (nm)	d$_s$ (nm)
KIT-6-30	7.79	625.46	0.5668	3.88	3.91
KIT-6-50	7.98	515.25	0.5608	4.67	3.31
KIT-6-80	8.59	611.28	0.8829	5.89	2.70
KIT-6-100	9.05	763.54	1.2589	6.62	2.43
KIT-6-120	9.31	519.52	1.2131	8.95	0.36
KIT-6-180	9.31	297.59	1.4396	18.57	–

Fig. 4. Peak-normalized positron lifetime spectra measured for KIT-6 at synthesis temperature of 30 °C, 100 °C and 180 °C.

The two long lifetimes τ_3 (∼5 ns) and τ_4 (75–105 ns) are obviously the o-Ps lifetime in micropores and mesopores, respectively.

According to the Tao-Eldrup model (Eq. (1)), the size of micropore can be estimated from the lifetime τ_3, which is about 0.95 nm in diameter. These micropores exist in the silica wall and provide interconnections for adjacent mesopores. Wang et al. [44] obtained the micropore volume of KIT-6 from nitrogen adsorption/desorption measurements, but they did not show the micropore diameter. This might be due to the difficulty in obtaining the reliable size of very small micropores in silica materials from the nitrogen adsorption/desorption isotherm [45].

The size of mesopores can be also obtained from the longest lifetime τ_4. However, since the mesopore is larger than 2 nm, the self-annihilation of o-Ps through 3γ emission should be considered. Ito et al. extended Tao-Eldrup model by taking into consideration the self-annihilation of o-Ps through three gamma annihilation [24]. They still use a spherical infinite potential-well model, and the relationship between o-Ps lifetime and pore size is as follows:

$$\tau_{o-Ps}^{-1} = 2\left[1 - \frac{R_a}{R_a + \Delta R} + \frac{1}{2\pi}\sin\left(\frac{2\pi R_a}{R_a + \Delta R}\right)\right]\left[1 - \left(\frac{R - R_a}{R + \Delta R}\right)^b\right] + \frac{1}{142},$$
(5)

where R_a = 0.88 nm and b = 0.55 are fitted parameters, and the last item 1/142 is the self-annihilation rate of o-Ps [24].

Besides the Ito's model, other extended models to correlate o-Ps lifetime with pore size for different pore geometry. Dull et al. extended Tao-Eldrup models for rectangular tube [21,25]:

$$\lambda(T) = \lambda_A - \frac{\lambda_S - \lambda_T}{4}F(a,\delta,T)F(b,\delta,T)F(c,\delta,T),$$
(6)

$$F(x,\delta,T) = 1 - \frac{2\delta}{x} + \frac{\sum_{i=1}^{\infty}(1/(i\pi))\sin((2i\pi\delta)/x)e^{((-\beta t^2)/(x^2 kT))}}{\sum_{i=1}^{\infty}e^{((-\beta t^2)/(x^2 kT))}},$$
(7)

where $\beta = h^2/(16\,\text{m}) = 0.188$ eV nm^2.

Goworeck et al. also proposed a new model for pores with shape of cylindrical tube [26]. By using the above three models, the size of mesopore synthesized at 30 °C is about 5.73 nm, 2.82 nm and 4.21 nm, respectively. The pore size from Ito's model is overestimated, while it is underestimated from Dull's model. Only the pore size calculated from Goworeck's model is closest to the size obtained by N$_2$ adsorption measurement, which is about 3.88 nm. This suggests that the mesopore is cylindrical.

Fig. 5 shows variation of the two long lifetimes τ_3 and τ_4 and their intensities I$_3$ and I$_4$ for KIT-6 synthesized at the different
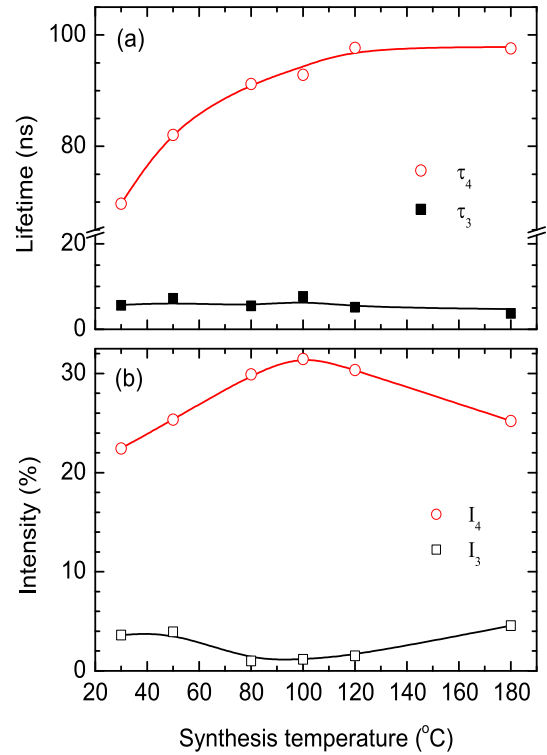
Fig. 5. Variation in the two long lifetimes τ_3 and τ_4 and their intensities I$_3$ and I$_4$ for KIT-6 synthesized at different hydrothermal temperatures.

hydrothermal temperature. τ_3 is almost constant at about 5 ns. This suggest that the increase of hydrothermal temperature has no effect on the micropore sizes of KIT-6. The longest lifetime τ_4 shows continuous increase with increasing synthesis temperature, which indicates the increase of mesopore size. This is in agreement with N$_2$ adsorption/desorption measurement and also HRTEM observation. The intensity of long lifetime components I$_3$ and I$_4$ may reflect the relative number of micropores and mesopores. From Fig. 5 we can note that I$_4$ increases from 22% to 31% and I$_3$ with increasing synthesis temperature from 30 °C to 100 °C, and then begins to decrease and it drops abruptly to about 25% at 180 °C. This is a clear indication of the collapse of ordered mesopore structure at 180 °C, and some neighboring pores combine into larger mesopores or even macropores. The variation of intensity I$_3$ is contrary to that of I$_4$, which first show continuous decreases from about 3.9% to 1.1% with increasing synthesis temperature up to 100 °C, then increases from 1.1% to 4.5% with increasing temperature. The decrease of I$_3$ in the first stage means decrease of the relative number of micropores, which is related to the decrease of wall thickness with increasing hydrothermal treatment temperature as described above, since the micropore are inside the pore wall. Wang et al. [44] also observed the decrease of micropore volume for the KIT-6 with higher hydrothermal treatment temperature. The later increase of I$_3$ in the temperature range of 120–180 °C is most probably due to the formation of additional micropores due to the collapsed of the ordered mesopore structure.

The mesopore sizes at different synthesis temperatures were calculated from the o-Ps lifetime τ_4 using Ito, Dull and Goworeck's model, respectively, and the result is compared with that of N$_2$ adsorption/desorption measurement. From Fig. 6, it can be seen that the pore sizes calculated by Goworeck's cylindrical model are in good agreement with N$_2$ adsorption/desorption measurement as the synthesis temperature is in the range of 30–120 °C. However, for the sample synthesized at 180 °C, the pore sizes calculated by the three model are all smaller than N$_2$
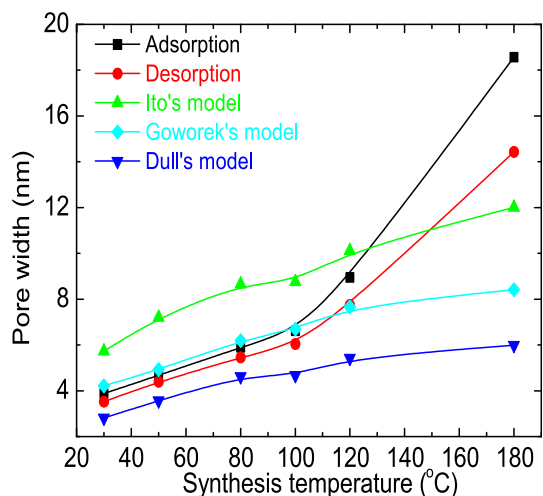
Fig. 6. Pore radius of KIT-6 attained from N$_2$ adsorption/desorption and PAL measurements using different model.

adsorption/desorption measurement. This indicates that the mesopores in samples synthesized at 30–120 °C are typical cylindrical pores. At higher hydrothermal temperatures, the underestimation of the pore size obtained by positron annihilation is probably due to the change of pore morphology after hydrothermal treatment at high temperatures. There is another possibility that due to the decrease in the wall thickness, the interconnection of neighboring mesopores will be recognized as larger pores by N$_2$ sorption method, while positron still discriminate the two neighboring pores as individual pores.

Since the second lifetime τ_2 is the annihilation lifetime of positrons trapped at pores, it can also reflect the change of pore size with increasing synthesis temperature of the samples. Fig. 7 shows positron lifetime τ_2 and o-Ps lifetime τ_4 of samples synthesized at different temperatures. It is interesting to note that both τ_2 and τ_4 increase as a function of synthesis temperature with nearly the same trend. This reveals two facts. First, the lifetime τ_2 and o-Ps lifetime τ_4 reflect microstructural information from the same site, which is inside the mesopore. Second, the lifetime τ_2 can also be used to characterize pore size in mesoporous materials. This idea has been proposed by Jean et al. [35] in polymeric materials. However at present no appropriate model is available to correlate τ_2 with mesopore size.

It is generally believed that if positron lifetime is longer than 500 ps, it is most probably due to formation and annihilation of
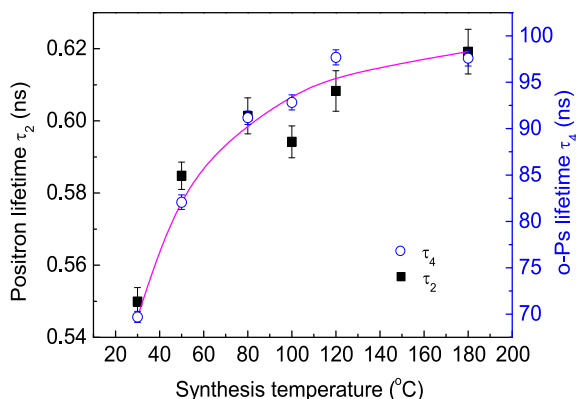

Fig. 7. Positron lifetime τ_2 and o-Ps lifetimes τ_4 of samples synthesized at different temperatures.
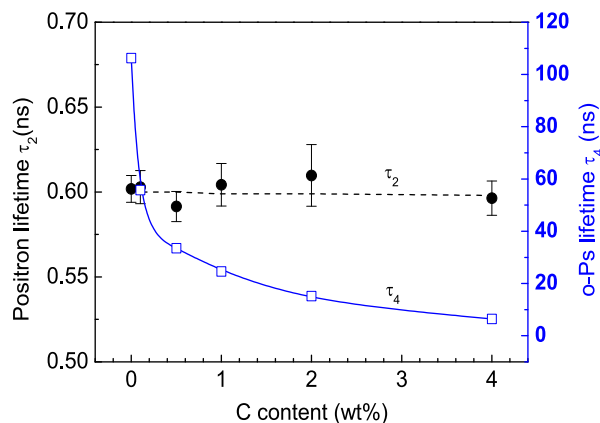

Fig. 8. Variation of positron lifetime τ_2 and o-Ps lifetime τ_4 as a function of carbon content in C/SBA-15 complex.

positronium, especially the pick-off annihilation of o-Ps lifetime. In other words, the upper limit of positron lifetime in the trapped state is suggested to be 500 ps. However, lifetime τ_2 in the present work is in the range of 549–619 ps. If it is due to o-Ps annihilation, the pores where o-Ps resides will be very small, which will have little chance to expand with the same trend as the mesopore. Therefore we believe that τ_2 is not due to o-Ps annihilation.

There are a lot of published papers which reported positron lifetime longer than 500 ps in pores or free volume holes [32,35,46,47]. If such lifetime is due to the o-Ps annihilation, it will also has quenching effect or chemical reaction induced by some active substance. In our recent paper we observed the strong inhibition of positronium formation by carbon in porous γ-Al$_2$O$_3$, which has also been observed by Wawryszczuk et al. [27] in mesoporous MCM-41. The conductive carbon will cause decrease in both o-Ps lifetime and its intensity. However, we did not find any change in the second lifetime τ_2. In order to further verify that the lifetime τ_2 in ordered mesoporous materials is the lifetime of positron trapped in mesopores rather than o-Ps annihilation lifetime, we prepared another mesoporous SBA-15, and filled it with different amount of carbon. Different amounts of sucrose as the carbon source were immersed in SBA-15. The mixture were placed in an oven and was kept at 100 °C for 6 h and then 160 °C or another 6 h for pre carbonization. Finally, the samples were calcined at 900 °C under vacuum for complete carbonization. Thus a series of C/SBA-15 composites were obtained with C content ranging from 0 wt% to 4 wt%. The C content was calculated from the sucrose added. Fig. 8 shows the variation of positron lifetime τ_2 and o-Ps lifetime τ_4 as a function of C content. τ_4 shows very rapid decrease from 106 ns to about 6 ns with carbon content increasing from 0 wt% to 4 wt%, and the corresponding intensity I$_4$ decrease to zero at carbon content of 4 wt%. This indicates strong quenching and inhibition effect on positronium formation and annihilation. However, τ_2 keeps almost unchanged. This confirms that τ_2 is the annihilation of positron in pores. It also implies that even the positronium formation is completely forbidden in some porous materials, we can still use lifetime τ_2 to characterize the pore structure.

4. Conclusion

In summary, mesoporous KIT-6 was synthesized at different temperatures. SAXS, HRTEM and N$_2$ adsorption/desorption measurements confirm the ordered mesoporous structure with cubic Ia3d symmetry, and the pore size can be tuned from 3.8 nm to 8.9 nm by varying the synthesis temperature from 30 °C to

120 °C. At the same time, the wall thickness shows gradual decrease with increasing synthesis temperature. Positron lifetime measurements reveal two kinds of pores: the micropore and mesopore. With increasing synthesis temperature from 30 °C to 120 °C, the size of micropore is kept at around 0.9 nm, while the mesopore size based on Goworeck's model increases from 4.2 nm to 7.7 nm. Due to the decrease of wall thickness, the number of micropores shows decrease with increasing synthesis temperature. The pore order is deteriorated at synthesis temperature of 180 °C, and the pore size was estimated to be 18.6 nm and 8.4 nm by N_2 adsorption/desorption and positron lifetime measurements, respectively. It was found that the positron lifetime τ_2 can also reflect the pore size, which increases with the same trends as *o*-Ps lifetime τ_4. Our results confirm that positron is a sensitive and nondestructive probe for the pore structure in KIT-6, and the pore size can be tailored by changing the hydrothermal temperature during synthesis of the sample.

Acknowledgments

References

[1] J. Fan, C.Z. Yu, F. Gao, J. Lei, B.Z. Tian, L.M. Wang, Q. Luo, B. Tu, W.Z. Zhou, D.Y. Zhao, Angew. Chem. 116 (2003) 3254–3258.

[2] H. Song, R.M. Rioux, J.D. Hoefelmeyer, R. Komor, K. Niesz, M. Grass, P.D. Yang, G.A. Somorjai, J. Am. Chem. Soc. 128 (2006) 3027–3037.

[3] Z.Y. Zhang, F. Zuo, P.Y. Feng, J. Mater. Chem. 20 (2010) 2206–2212.

[4] D. Gu, F. Schuth, Chem. Soc. Rev. 43 (2014) 313–344.

[5] D.Y. Zhao, Q.S. Huo, J.L. Feng, B.F. Chmelka, G.D. Stucky, J. Am. Chem. Soc. 120 (1998) 6024–6036.

[6] D.Y. Zhao, J.Y. Sun, Q.Z. Li, G.D. Stucky, Chem. Mater. 12 (2000) 275–279.

[7] D.Y. Zhao, J.L. Feng, Q.S. Huo, N. Melosh, G.H. Fredrickson, B.F. Chmelka, G.D. Stucky, Science 279 (1998) 548–552.

[8] J. Lee, S.H. Joo, R. Ryoo, J. Am. Chem. Soc. 124 (2002) 1156–1157.

[9] X.Q. Wang, Y. Zhang, W. Luo, A.A. Elzatahry, X.W. Cheng, A. Alghamdi, A.M. Abdullah, Y.H. Deng, D.Y. Zhao, Chem. Mater. 28 (2016) 2356–2362.

[10] C.F. Cheng, W.Z. Zhou, J. Klinowski, Chem. Phys. Lett. 263 (1996) 247–252.

[11] Y. Meng, D. Gu, F.Q. Zhang, Y.F. Shi, H.F. Yang, Z. Li, C.Z. Yu, B. Tu, D.Y. Zhao, Angew. Chem. 117 (2005) 7215–7221.

[12] J. Fan, C.Z. Yu, J. Lei, Q. Zhang, T.C. Li, B. Tu, W.Z. Zhou, D.Y. Zhao, J. Am. Chem. Soc. 127 (2005) 10794–10795.

[13] F. Kleitz, S.H. Choi, R. Ryoo, Chem. Commun. (2003) 2136–2137.

[14] Y. Doi, A. Takai, Y. Sakamoto, O. Terasaki, Y. Yamauchi, K. Kuroda, Chem. Commun. 46 (2010) 6365–6367.

[15] A. Dupasquier, A.P. Mills Jr, Positron Spectroscopy of Solids, IOS Press, Amsterdam, 1995.

[16] Krause-Rehberg, R. Leipner, H.S., Positron Annihilation in Semiconductors, Defect Studies, Springer Series in Solid-State Sciences, vol. 127, Berlin, 1999.

[17] Y.C. Jean, P.E. Mallon, D.M. Schrader Principles and Application of Posiron and Positronium Chemistry, World Scientific, Singapore, 2003.

[18] J. Lahtinen, P. Hautoj Rvi, J. Phys. Chem. B 101 (1997) 1609–1614.

[19] S.J. Tao, J. Chem. Phys. 56 (1972) 5499–5510.

[20] M. Eldrup, D. Lightbody, J.N. Sherwood, Chem. Phys. 63 (1981) 51–58.

[21] T.L. Dull, W.E. Frieze, D.W. Gidley, J.N. Sun, A.F. Yee, J. Phys. Chem. B 105 (2001) 4657–4662.

[22] R. Zaleski, J. Wawryszczuk, T. Goworek, Radiat. Phys. Chem. 76 (2007) 243–247.

[23] S. Thranert, D. Enke, G. Dlubek, R. Krause-Rehberg, Mater. Sci. Forum 607 (2009) 169–172.

[24] K. Ito, H. Nakanishi, Y. Ujihira, J. Phys. Chem. B 103 (1999) 4555–4558.

[25] D.W. Gidley, W.E. Frieze, T.L. Dull, A.F. Yee, E.T. Ryan, H.M. Ho, Phys. Rev. B 60 (1999) R5157–R5160.

[26] T. Goworek, K. Ciesielski, B. Jasinska, J. Wawryszczuk, Chem. Phys. 230 (1998) 305–315.

[27] J. Wawryszczuk, J. Goworek, R. Zaleski, T. Goworek, Langmuir 19 (2003) 2599–2605.

[28] A. Sousa, K.C. Souza, S.C. Reis, R.G. Sousa, D. Windmoller, J.C. Machado, E.M.B. Sousa, J. Non-Cryst. Solids 354 (2008) 4800–4805.

[29] M. Koshimizu, K. Shimokita, H.S. Zhou, I. Honma, K. Asai, J. Phys. Chem. C 112 (2008) 8779C8783.

[30] H.J. Zhang, Z.Q. Chen, S.J. Wang, A. Kawasuso, N. Morishita, Phys. Rev. B 82 (2010) 035439.

[31] M. Gorgol, R. Zaleski, A. Kierys, Nukleonika 58 (2013) 229–233.

[32] C.Y. Li, N. Qi, Z.W. Liu, B. Zhou, Z.Q. Chen, Z. Wang, Appl. Surf. Sci. 363 (2016) 445–450.

[33] T. Hyodo, T. Nakayama, H. Saito, F. Saito, K. Wada, Phys. Stat. Sol. (c) 6 (2009) 2497–2502.

[34] C.Y. Li, B. Zhao, B. Zhou, N. Qi, Z.Q. Chen, W. Zhou, Phys. Chem. Chem. Phys. 19 (2017) 7659–7667.

[35] K.S. Liao, H.M. Chen, S. Awad, J.P. Yuan, W.S. Hung, K. Lee, J. Lai, C. Hu, Y.C. Jean, Macromolecules 44 (2011) 6818–6826.

[36] E.P. Barrett, L.G. Joyner, P.P. Halenda, J. Am. Chem. Soc. 73 (1951) 373–380.

[37] C. Pirez, J.M. Caderon, J.P. Dacquin, A.F. Lee, K. Wilson, Acs. Catal. 2 (2012) 1607–1614.

[38] R. Kishor, A.K. Ghoshal, Micropor. Mesopor. Mat. 242 (2017) 127–135.

[39] M. Thommes, K. Kaneko, A.V. Neimark, J.P. Olivier, F. Rodriguez-Reinoso, J. Rouquerol, K.S. Sing, Pure. Appl. Chem. 87 (2015) 1051–1069.

[40] R. Schmidt, E.W. Hansen, M. Stoecker, D. Akporiaye, O.H. Ellestad, J. Am. Chem. Soc. 117 (1995) 4049–4056.

[41] M.E. Davis, Nature 417 (2002) 813–821.

[42] P. Kirkegaard, N.J. Pederson, M. Eldrup, PATFIT-88: A Data-Processing System for Positron Annihilation Spectra on Mainframe and Personal Computers, 1989.

[43] H. Saito, T. Hyodo, Phys. Rev. Lett. 90 (2003) 193401.

[44] W. Wang, R. Qi, W.J. Shan, X.Y. Wang, Q.L. Jia, J. Zhao, C.P. Zhang, H.Q. Ru, Micropor. Mesopor. Mat. 194 (2014) 167–173.

[45] K. Kaneko, J. Membr. Sci. 96 (1994) 59–89.

[46] A.M. Habrowska, E.S. Popiel, J. Appl. Phys. 62 (1987) 2419–2423.

[47] C.H. Lo, K.S. Liao, W.S. Hung, M.D. Guzman, C.C. Hu, K. Lee, J. Lai, Micropor. Mecopor. Mat. 141 (2011) 140–145.